Food & Function

ROYAL SOCIETY OF CHEMISTRY

PAPER

View Article Online
View Journal | View Issue

Cite this: *Food Funct.*, 2025, **16**, 6898

Design, synthesis and evaluation of gluten peptide analogues as inhibitors of the HLA/DQ8-mediated celiac immune response†

Lucia Treppiccione, [a] Vincenzo Mangini, [b] Annarita Del Gatto,*[c,d] Daniela Trisciuzzi,[e] Francesco Maurano,[a] Anna Giovanna Sciancalepore,[b] Laura Zaccaro,[c] Benny Danilo Belviso, [b] Orazio Nicolotti,[e] Michele Saviano, [f] Mauro Rossi[a] and Rocco Caliandro *[b]

The immune response induced by gluten is the result of molecular mechanisms involving gliadin peptides, DQ2 or DQ8 glycoproteins, and the interaction with T lymphocyte receptors. DQ8-glia-α1 is an immunodominant peptide present in gliadin from wheat *Triticum spelta* that interacts with the DQ8 protein, as proven through transgenic mouse models. The research was carried out by performing a computational analysis aimed at finding antagonistic peptides of the DQ8-glia-α1 peptide, *i.e.* peptides obtained by varying its amino acids to maintain or even enhance the binding towards DQ8 and at the same time to prevent an immune response by a reduced interaction with the T lymphocyte receptors. Crystallographic structures of DQ8 and three different T-cell receptors were taken as experimental starting systems, the peptide–protein interaction was modelled by molecular dynamics simulations and molecular interaction field calculations, and the optimal mutations of the peptide sequence were identified by using multivariate analysis. The method provided a list of nine immunodominant peptide candidates, which were produced by chemical synthesis and validated by tests on transgenic mice. The results showed that immunization with the peptide (DQ8-glia-α1, designated M1) induced *in vitro* antigen-specific secretion of IFN-γ restricted to the M1 peptide alone. M1 also stimulated antigen-specific secretion of the regulatory cytokine IL-10. A peptide (*i.e.*, M10) was identified as a potential therapeutic molecule for down-regulating the inflammatory condition triggered by the DQ8-glia-α1 immunodominant peptide in CD.

Received 12th March 2025,
Accepted 24th July 2025

DOI: 10.1039/d5fo01270h

rsc.li/food-function

1 Introduction

Coeliac disease (CD) is a widespread food-related and immune-related disorder triggered by wheat gluten (gliadins and glutenins). The human leucocyte antigen (HLA)-DQ2/HLA-DQ8 heterodimers are expressed in almost all CD patients, suggesting a major role of adaptive immunity in CD pathogenesis.[1] In particular, it has been shown that gliadin-specific $CD4^+$ T lymphocytes produce high levels of IFN-γ, an inflammatory cytokine, in the small intestine, following site-specific deamidation of wheat gliadin by tissue transglutaminase (tTG).[2] We have previously shown that gliadin induced a similar antigen-specific T cell response in HLA-DQ8 (DQ8) transgenic mice with high levels of IFN-γ.[3,4] DQ8 mice represent a useful model for CD analysis because they express the CD-related HLA-DQ8 molecule on the surface of immune competent cells in the absence of any endogenous mouse class II heterodimer.[5]

On the other hand, several gliadin epitopes have been identified[6] and a specific gliadin peptide has been described to be immunodominant in DQ8 adults.[7] It is the HLA-DQ8-restricted immunodominant gliadin peptide DQ8-glia-α1 from the wheat *Triticum spelta* (SGEGSFQPSQENP), which will be hereafter denoted as M1.[8]

In this study, we aim at identifying immunodominant synthetic peptides derived from M1 which, unlike this one, do not trigger the immune response typical of CD. Given the large chemical space to explore, we preferred to adopt a comprehen-

[a]*Institute of Food Sciences, National Research Council, Avellino, Italy*
[b]*Institute of Crystallography, National Research Council, Bari, Italy.*
E-mail: rocco.caliandro@cnr.it
[c]*Institute of Biostructures and Bioimaging, National Research Council, Napoli, Italy.*
E-mail: annarita.delgatto@cnr.it
[d]*Interuniversity Research Centre on Bioactive Peptides (CIRPeB) "Carlo Pedone", University of Naples "Federico II", Naples, Italy*
[e]*University of Bari Aldo Moro, Bari, Italy*
[f]*Institute of Crystallography, National Research Council, URT, Caserta, Italy*

†Electronic supplementary information (ESI) available: PDB files of the atomistic models of the DQ8/DQ8-glia-α1 complex for each of the mutation applied to the peptide. See DOI: https://doi.org/10.1039/d5fo01270h

sive computational approach based on systematic application of point mutations to M1, followed by molecular dynamics (MD) and estimation of binding energy with two complementary calculations. The best candidates have been produced and validated by the murine model described above.

2 Materials and methods

2.1 Design of synthetic gliadin peptides

The experimental structural models of DQ8 in a complex with the immunodominant gliadin peptide DQ8-glia-α1 are reported in Table 1.

A comparative structural analysis between the structural models reported in Table 1 highlights a very good overlap for the DQ8 protein and the DQ8-glia-α1 interacting peptide (RMSD < 1 Å), while the interaction of the T-cell receptors is characterized by greater variability, mainly depending on the type of receptor (Fig. 1). Structural knowledge is available for the human receptors S13,[8] L3–12[8] and Bel502 (UniProt A0A0B4J274),[9] included respectively in the crystal structures with the PDB codes 4Z7U, 4Z7V and 5KS9. Furthermore, by comparing the configuration of the peptide in the 2NNA model (in pink in Fig. 1) and that in the remaining structures (in blue in Fig. 1), it can be concluded that it is only weakly influenced by the presence of the T-cell receptor. A more in-depth analysis revealed that the α and β chains of S13 and L3–12 have the same sequence and similar three-dimensional arrangements. Moreover, the 4GG6 structure was not considered, due to the low resolution of its X-ray diffraction data. Therefore, among the structures reported in Table 1, the 2NNA model was taken as a representative of the interaction between the DQ8-glia-α1 peptide and the DQ8 protein, and the 4Z7U, 4Z7W and 5KS9 models as a representative of the interaction between the DQ8-glia-α1 peptide, the DQ8 protein and the T-cell receptor.

In light of the above considerations, and of the current knowledge about the immune response to gluten peptides, a protocol has been prepared for a comprehensive computational analysis, aimed at designing antagonistic peptides of the DQ8-glia-α1 peptide, *i.e.* peptides obtained from it by varying its amino acids that are able to maintain or even enhance the binding towards DQ8 and at the same time to prevent the triggering of an immune response by a reduced interaction with the T lymphocyte receptors. The analysis strategy used herein is summarized in Fig. 2, exploiting MD simulation as a computational investigation tool; the 2NNA, 4Z7U, 4Z7W and 5KS9 crystallographic structures as experimental starting systems; and the systematic execution of mutations in the peptide sequence as a method to explore the peptide variants.

2.1.1 Molecular dynamics simulations. MD calculations were performed following a protocol appropriately calibrated on the system under study, which involves the execution of an energy minimization for 10 ps, followed by heating for 20 ps, during which the positions of the atoms involved in the peptide bond are restrained using a spring constant of 0.5 kcal mol^{-1}. Finally, the structure undergoes MD in the explicit solvent for 100 ps. Coordinates were saved at regular time intervals of every 2 ps. MD simulations with short timeframes were intended to explore the local conformational changes induced by the mutated residues of the peptides already bound to DQ8 and T-cell receptors, with the aim of improving comparative energy calculations. The study of the pre-binding behaviour of the free peptides,[11,12] which would have required larger timeframes, has not been considered in this study.

Table 1 Crystal structures containing DQ8 in the complex with the gliadin peptide DQ8-glia-α1

PDB code	Content	Data resolution (Å)
2NNA	DQ8, DQ8-glia-α1	2.10
4Z7U	DQ8, DQ8-glia-α1, T-cell receptor S13	2.70
4Z7V	DQ8, DQ8-glia-α1, T-cell receptor L3–12	2.65
4Z7W	DQ8, DQ8-glia-α1, T-cell receptor T316	2.89
4GG6	DQ8, DQ8-glia-α1, T-cell receptor SP3.4	3.20
5KS9	DQ8, DQ8-glia-α1, T-cell receptor Bel502	2.55

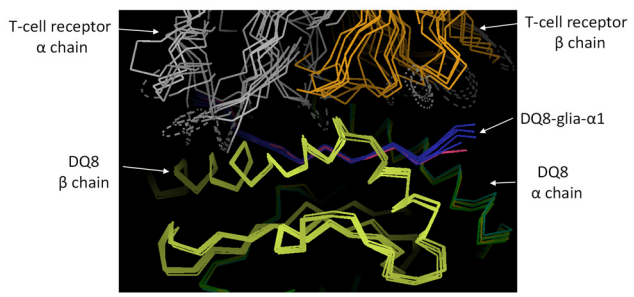

Fig. 1 Overlay of the crystal structures reported in Table 1, with details of the interaction region between the DQ8-glia-α1 peptide, the DQ8 protein (a heterodimer composed of the α and β chains encoded by the DQA1 and DQB1 genes, respectively) and the T-cell receptor. All proteins are represented using C_α tracing. Missing loops are shown as dashes. The peptide present in the 2NNA structure is shown in magenta. The figure was prepared by using the Coot program.[10]

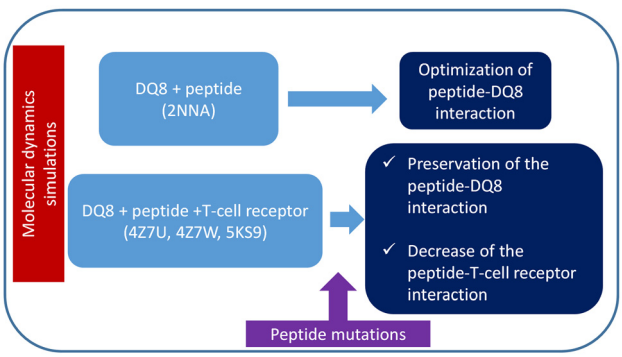

Fig. 2 Strategy for the identification of DQ8-glia-α1 antagonist peptides through computational modelling.

The computer program NAMD[13] was used, with the CHARMM (PARAM36) force field[14] for protein atoms, the Beglov and Roux force fields for chlorine counterions[15] and the TIP3P model[16] for water molecules. Long-range electrostatic interactions were treated with the particle mesh Ewald method.[17] A Fourier spacing of 0.12 nm combined with a fourth-order cubic spline interpolation was used. A 1.2 nm cut-off was used for van der Waals interactions, as well as for the real-space part of the electrostatic interactions. All bond lengths with hydrogens were constrained with the SHAKE algorithm[18] and the time step was set to 2 fs. NPT ensemble (T = 298 K, P = 1 bar) MD simulations were carried out by coupling the systems with a Nose–Hoover thermostat[19] and an Andersen–Parrinello–Rahman barostat.[20,21]

Each of the 13 amino acids constituting the DQ8-glia-α1 peptide was systematically varied for each of the 20 natural amino acids, by using a PyMOL[22] script, resulting in 13 × 19 = 247 single-mutation peptides that have been evolved through MD simulations. Additional simulations were performed to investigate multiple mutations of the DQ8-glia-α1 peptide, implemented by using the mutator tool of VMD.[23]

Calculations were performed at the CINECA supercomputer facility GALILEO100, through the ELIXIR-IT HPC@CINECA initiative.[24]

2.1.2 Analysis of the MD data. For each MD run, the interaction energy between the peptide and the DQ8 protein averaged during the simulation time was calculated. It depends on the mutual position of the peptide and protein atoms and includes energy terms due to van der Waals and electrostatic forces. The difference between the energy values obtained for each single mutation compared to that obtained for the native peptide (ΔE) was taken as a benchmark parameter to optimize the DQ8–peptide interaction. Calculations were performed by using the computer program VMD.[23]

Interaction energy profiles along the peptide residues, calculated from the MD data by summing the energies of the residue atoms for the last frame, were representative of each simulated system. They have been compared by Principal Component Analysis (PCA), followed by hierarchical clustering by using the RootProf program.[25] Energy profiles were rescaled by the standard normal variate, so that they all have the same mean and standard deviation. Only two principal components have been considered, as for most of the cases they explained more than 60% of the cumulative data variance. An unsupervised hierarchical clustering was carried out on the PCA score values of the top-two principal components, by using group average as linkage metrics.

2.1.3 Molecular interaction fields. An alternative calculation of the binding interaction energy has been carried out by using the GRID force field implemented into BioGPS software developed and licensed by Molecular Discovery Ltd (**https://www.moldiscovery.com**). The GRID force field was able to evaluate the type, strength and direction of the molecular interactions established between macromolecules by employing molecular interaction fields (MIFs) based on hydrophobic, HB acceptor, and HB donor probes as elsewhere reported.[26–28] The total computed is thus given as a linear combination of such energetic terms. Based on the last frame of the MD simulations devoid of water molecules, we computed the difference of the interaction energy (*i.e.* ΔE) for the systems formed by the DQ8 protein *vs.* the mutated/native DQ8-glia-α1 peptide. The computed values of ΔE were compared to the data acquired through MD simulations.

2.2 Peptide synthesis and characterization

2.2.1 Materials. Polypropylene reaction vessels and sintered polyethylene frits were supplied by Biotage AB (Uppsala, Sweden), NovaSyn TGA resin, 2-(1*H*-benzotriazole-1-yl)-1,1,3,3-tetramethyluronium hexafluorophosphate (HBTU), cyano-hydroxyimino-acetic acid ethyl ester (Oxyma) and all amino acids were from Novabiochem-Merck (Nottingham, UK). Kaiser test, 1-(mesitylene-2-sulfonyl)-3-nitro-1,2,4-triazole (MSNT), 1-methylimidazole (MeIm), *N*,*N*-dimethylformamide (DMF), *N*,*N*-0-diisopropylethylamine (DIPEA), piperidine, trifluoroacetic acid (TFA), and scavengers 1,2-ethanedithiol (EDT) and triisopropylsilane (TIS) and human serum (Lonza, Basel, Switzerland) were purchased from Sigma-Aldrich (Milan, Italy). *N*-Methyl-2-pyrrolidone (NMP) was purchased from CARLO ERBA Reagents (Milan, Italy). Acetonitrile (ACN), dichloromethane (DCM) and diethyl ether were purchased from VWR International (Milan, Italy). All aqueous solutions were prepared by using water obtained from an Arium® Pro Ultrapure Water System (Sartorius, conductivity: 0.055 μS cm^{-1} (≅18.2 MΩ cm); TOC content: <5 ppb; bacteria: <0.001 CFU mL^{-1}; no particles: >0.22 μm).

2.2.2 Methods. All peptides were manually synthesized by the Fmoc solid-phase strategy (scale: 0.1 mmol). The syntheses were performed on a NovaSyn TGA resin (substitution: 0.29 mmol g^{-1}) by using all standard amino acids and polypropylene reaction vessels fitted with sintered polyethylene frits. Activation of the resin with the first amino acid was performed by treating the solid support with Fmoc-Gln(Trt)-OH (5 equiv.)/MSNT (5 equiv.)/MeIm (3.75 equiv.) in anhydrous DCM for 90 min. The resin activation percentage was determined spectroscopically by treating the peptidyl-resin with a 30% piperidine solution in DMF for 5 min, by evaluating the adsorption at 301 nm of the Fmoc-piperidine adduct (dibenzofulvene) formed and calculating its concentration.

Deprotection reactions were performed by removing the Fmoc protecting group with 30% piperidine in DMF (3 × 10 min). Coupling reactions were carried out by using 10 equiv. of Fmoc-protected amino acids activated *in situ* with HBTU (9.8 equiv.)/Oxyma (9.8 equiv.) in DMF and DIPEA (20 equiv.) in NMP for 1 h. The coupling efficiency was assessed by the qualitative Kaiser test.

Once the syntheses were completed, the peptides were cleaved off the resin by treatment with a mixture of TFA/H_2O/EDT/TIS (94 : 2.5 : 2.5 : 1, v/v/v/v) for 3 h at room temperature, under stirring. The resin was then filtered, and the crude peptides were precipitated with cold diethyl ether dissolved in a H_2O/ACN solution and freeze-dried.

Crude products were purified by preparative RP-HPLC using an Agilent Technologies PrepStar system equipped with a

G9309A 325 UV-Vis dual wavelength detector, an Aeris peptide XB-C18 column (250 × 21.2 mm; 5 μm; 100 Å), and a linear gradient of H_2O (0.1% TFA)/ACN (0.1% TFA) from 5% to 40% ACN (0.1% TFA) in 20 min at a flow rate of 20 mL min^{-1}. The collected fractions containing the peptides were then lyophilized.

The purity of the compounds was assessed by analysing the collected fractions by RP-HPLC. Particularly, an Agilent Technologies 1200 chromatographic system equipped with a diode array detector, an Aeris peptide XB-C18 column (100 × 4.6 mm; 3.6 μm; 100 Å) and a linear gradient of ACN from 5% to 70% (ACN dissolved in H_2O and 0.1% TFA) in 30 min at a flow rate of 1 mL min^{-1} were used. The identity of the compounds was confirmed by acquiring LC/MS mass spectra using an LC/MS Agilent single quadrupole system (Agilent 1260 Infinity II LC System) equipped with a diode array detector combined with a dual electrospray ion source, a single quadrupole mass analyzer and an Aeris peptide XB-C18 column (50 × 2.1 mm; 3.6 μm; 100 Å) at a flow rate of 200 μL min^{-1} and a linear gradient of ACN from 5% to 70% (ACN dissolved in H_2O and 0.05% TFA) in 12 min.

2.3 Serum stability assays

The proteolytic susceptibility of M1, M5 and M10 peptides was determined in a 10% (v : v) human serum (Lonza, Basel, Switzerland). Human serum was previously activated by cooling at 4 °C, centrifugation at 13 000*g* for 5 min and incubation at 37 °C for 10 min to eliminate the lipid fraction contained in it. Then, 50 μL of the serum was added to 250 μL of ultrapure water and 200 μL of 2.5 mg mL^{-1} peptide mother solution in ultrapure water, thus obtaining a final peptide concentration of 1 mg mL^{-1}. The mixture was incubated at 37 °C and after 1, 2, 4, 6, 8, 24, and 48 h, and the collected samples (25 μL) were centrifuged at 13 000*g* for 5 min and 20 μL of the supernatant was added to 80 μL of H_2O containing 0.05% TFA. Supernatants were finally analyzed by the LC/MS Agilent single quadrupole system (Agilent 1260 Infinity II LC System) equipped with a diode array detector combined with an electrospray ion source and a quadrupole mass analyzer using an Aeris peptide XB-C18 (100 × 4.6 mm; 3.6 μm; 100 Å) and a linear gradient of H_2O (0.05% TFA)/CH_3CN (0.05% TFA) from 5 to 70% of CH_3CN (0.05% TFA) in 30 min at a flow rate of 0.8 mL min^{-1}.

2.4 Mouse and antigen treatments

2.4.1 Preparation of pt-gliadin. Gliadin was extracted from commercial common wheat (*Triticum aestivum*) flour using a modified Osborne procedure[29] and freeze dried. 40 mg of gliadin was digested in 0.4 ml of 0.1 N HCl (pH 1.8) with pepsin (2500 units per mg; gliadin : enzyme 100 : 1; Merck Life Science S.r.l, Milan, Italy.) at 37 °C for 4 h in a shaking bath; the pH was increased at 8.0 and trypsin (2000 BAEE units per mg; gliadin : enzyme = 100 : 1; Merck Life Science S.r.l.) was added; the reaction was conducted at 37 °C for further 4 h and stopped by incubating in boiling water for 10 min; the digested gliadin (pt-gliadin) was freeze dried and stored at −80 °C.

2.4.2 *In vitro* treatment. AB^0 DQ8 transgenic mice expressing the HLA-DQ8 protein were reared on a gluten free diet (GFD) (Mucedola, SpA, Bolzano, Italy) at the mouse facility of the Institute of Food Sciences (accreditation no. 05/2024-UT). All procedures were performed in compliance with the ARRIVE guidelines, the EU Directive 2010/63/EU and institutional guidelines (Italian Ministry of Health, D.lgs. 26/2014). The Institutional Ethics Committee of Ministry of health (DGSAF) approved the study (approval number no.786/2024-PR). For the experiments, 6–12 weeks-old mice were administered intraperitoneally with M1 peptide or pt gliadin (100 μg) in 50 mM acetic acid. On day 14, the mice received a boost injection with the same amount of antigen. On day 24, the mice were sacrificed to collect the spleens.

2.4.3 *In vitro* cultures. Spleens were passed through a 40 μm cell strainer (Falcon, BD Biosciences, Erembodegem, Belgium) to dissociate the cells. To remove erythrocytes, spleen cells were suspended in a Tris-buffered ammonium chloride solution for 20 min at 4 °C. Then, cells were washed in a culture medium (RPMI 1640 containing 10% inactivated foetal calf serum, 100 U mL^{-1} penicillin, 100 μg mL^{-1} streptomycin, 1% non-essential amino acids, 2 mM glutamine, and 50 μM 2-mercaptoethanol). The cells were cultured at 1.5×10^6 cells per mL in 48-well flat bottom plates in the presence of ultra-filtered pt-gliadin, M1, analogue peptides (200 μg mL^{-1}) or a combination of equimolar amounts of M1 and analogues. After 72 h, the supernatants were collected and analysed for IFN-γ and IL-10 protein levels by sandwich-type ELISA or stored at −80 °C for multiplex analysis.

2.4.4 Multiplex analysis. Culture supernatants were assayed using a Luminex 200 analyser (Luminex Corporation, Austin, TX, USA) using a custom mouse cytokine/chemokine magnetic bead premixed 7-plex kit (ProcartaPlex Mix&Match 7-plex). The kit enabled the simultaneous quantification of the following molecules: IFN-γ, IL-6, TNF-alpha, IL-10, IL-17A, IL-4 and IL-21. Quantitative results were determined from the standard curve using xPONENT® 4.2, a logistic four-parameter curve fit software (DiaSorin Corporate, Saluggia-VC, Italy).

2.4.5 Statistical analysis. The ELISA results were evaluated by the Kruskal–Wallis test and Dunn's multiple comparisons test. The multiplex results were evaluated by one-way ANOVA and Tukey's multiple comparisons test. $P < 0.05$ was selected as the threshold of statistical significance.

3 Results

3.1 Identification of gliadin peptide mutations

As outlined in Fig. 2, the search for possible DQ8-glia-α1 antagonists has been divided in two steps, by optimizing first the interaction with DQ8, and then by hindering the interaction with the T-cell receptors.

3.1.1 Design of mutations for improving HLA/DQ8 binding. The crystallographic structure with the PDB code 2NNA, shown in Fig. 3, was used as a starting point for performing MD simulations. A visual analysis of Fig. 3 highlights

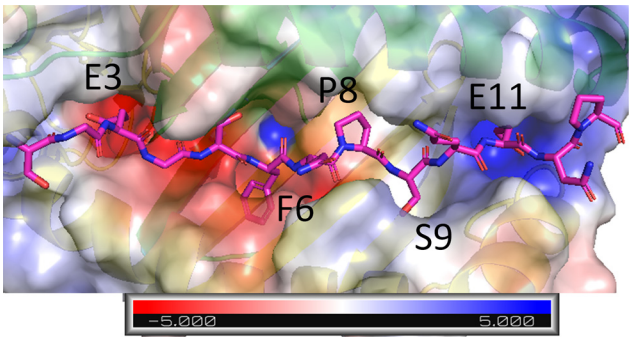

Fig. 3 Crystallographic structure (PDB code 2NNA) of the DQ8 heterodimer composed of α and β chains (green and yellow cartoons, respectively) interacting with the DQ8-glia-α1 peptide (shown with the stick representation). Electrostatic surface (+5 kT e^{-1}) obtained by the APBS tool[30] is shown. Peptide residues positioned in the interaction pockets with DQ8 (E3, F6, P8, S9 and E11) are labelled. The figure was prepared by using the PyMOL program.

that the amino acidic residues most involved in interactions with DQ8 are E3, F6, P8, S9 and E11.

The quantity of interest for this study was the energy difference Δ*E*, which highlights the ability of a given mutation in a given position of the DQ8-glia-α1 peptide to enhance (negative Δ*E* values) or worsen (positive Δ*E* values) the interaction between the peptide and the DQ8 protein. This difference, expressed in kcal mol^{-1}, is reported in Fig. 4.

It can be noted that residues E11 and E3 were characterized by positive Δ*E* for most of the mutations, suggesting that changing these residues reduces the interaction of the peptide with DQ8. In fact, these residues are known to be positioned in interaction pockets with DQ8.[31] Based on the simulations performed, it appears that these residues have higher Δ*E* for most of the mutations (Fig. 4). This evidence represents an important validation of the results of the MD, which can therefore be used to predict the mutations likely to improve the interaction of the peptide with DQ8.

From Fig. 4, it can also be seen that the most favorable mutations are those replacing short side-chain residues with long side-chain residues. Mutations with D, E, K or R, which are also ionizable residues at physiological pH, systematically have very low Δ*E* among all the residues of the peptide. In fact, by analyzing the final structures obtained from MD, it was possible to observe that the long side-chain amino acidic residues interacted more with the nearby residues of DQ8 and with solvent molecules present in the vicinity of the peptide. Apart from E3 and E11, amino acidic residues F6, P8 and S9 were involved in more than one interaction with DQ8 and were known to be positioned in DQ8 pockets.[32] Therefore, amino acidic residues E3, F6, P8, S9 and E11 were studied in detail, choosing among the mutations that stabilize the peptide + DQ8 system (those colored in blue in Fig. 4, mainly considering mutations towards long side-chain amino acidic residues) and performing the selected mutations simultaneously. Further simulations were then launched with multiple mutations, which produced the results shown in Fig. 5. Residue E11, which is essential to establish a peptide/protein interaction, given that no mutation performed produces a negative Δ*E* (Fig. 4), was not considered in the study of combined mutations.

It can be noted that the mutations on residues E3, F6, P8 and S9 towards long side-chain residues (K, E, D and D, respectively) produced clear decrements in the Δ*E* values. Such values were additive, meaning that the reductions obtained by performing all mutations simultaneously were nearly equal to the sum of the reductions obtained from single mutations. Importantly, the effects of these mutations were almost inde-

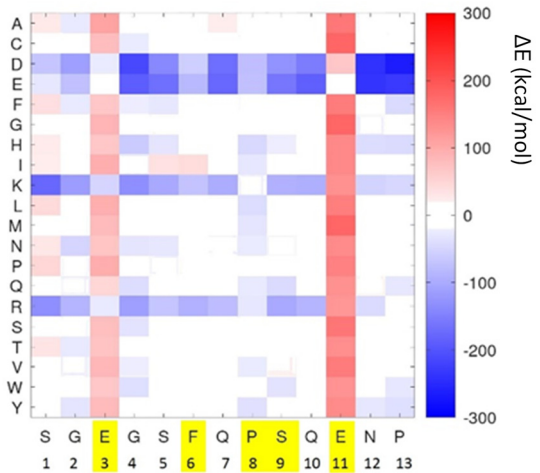

Fig. 4 Difference in the interaction energy Δ*E* calculated for the system composed of the mutated DQ8-glia-α1 peptide and the DQ8 protein with respect to the energy observed for the system with the native DQ8-glia-α1 peptide. Δ*E* is averaged along the simulation. Peptide residues (FASTA code and position) of DQ8-glia-α1 are shown in the *X*-axis, from the N-term to the C-term. *Y*-axis contains the mutated residues. The peptide residues most involved in interactions with DQ8 are highlighted in yellow. Negative Δ*E* values are in blue colour (stabilizing interaction) and positive Δ*E* values are in red colour (destabilizing interaction).

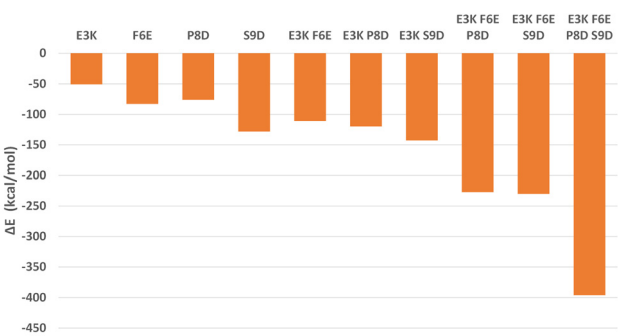

Fig. 5 Δ*E* values obtained by mutating the amino acidic residues of the DQ8-glia-α1 peptide most involved in interactions with DQ8: E3, F6, P8 and S9 (E11 was not subjected to mutations). The mutations were performed individually and in combination.

pendent, and each contributed to the interaction between the peptide and DQ8.

3.1.2 Study of the correlated effects among the mutations. Overall, MD results have been interpreted by using multivariate analysis applied on the residue-by-residue peptide energy profiles, which represent the effect of the mutation on the interaction between DQ8-glia-α1 and DQ8. In Fig. 6, each point represents the effect of a point-mutation on the peptide. The location of the point in the score plot depends on the characteristics of the corresponding energy profile. A clear separation can be noted among the representative points along the first principal component (PC1), which explains 59.3% of the total data variance. Points having negative PC1 values are all relative to the mutations of E11, and the energy profiles shown in the insets indicate that the effect of these mutations is a strong reduction of the interaction energy due to this residue. This confirms that any mutation of residue E11 worsens the interaction properties of the peptide with DQ8. Points having positive PC1 values can be divided into three clusters, among which the most populated is the one comprising mutations E3R, F6E, P8D and S9D. The features of the energy profiles belonging to this cluster are optimal, since they preserve the interaction energies at the E3 and E11 sites. Mutations located in the other two clusters can reduce or completely eliminate the E3 interaction pocket. For this reason, these mutations should be avoided. Such results confirm the validity of the chosen mutations E3R, F6E, P8D and S9D.

3.1.3 Design of mutations for reducing T-cell receptor binding. The previous analysis has allowed us to obtain the peptide M2: SGKGSEQDDQENP, which is supposed to have greater interactions with the DQ8 protein than the peptide M1. The underlined residues have already been optimized for this purpose, while the remaining ones are more involved in the interaction with the T-cell receptors, as can be seen in Fig. 7. These latter residues were subjected to a computational study based on MD simulations aimed at investigating the interaction with these receptors. MD simulations have been performed on the complexes between the T-cell receptor, DQ8 protein and selected peptides to assess which mutations of the peptide involved in the binding with the T-cell receptor worsen the interaction energy with respect to the DQ8 protein. Particularly, we exploited the crystal structures having the PDB code 4Z7U containing the T-cell receptor S13, 4Z7W containing the T-cell receptor L3–12, and 5KS9 containing the T-cell receptor Bel502 as the starting points of the simulations.

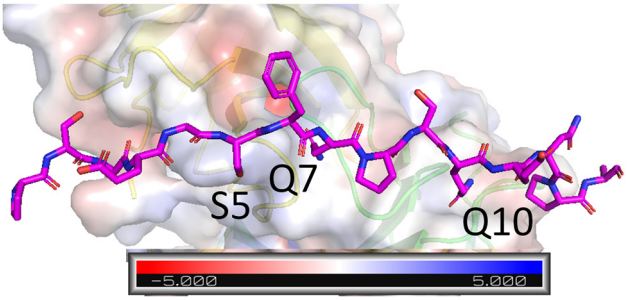

Fig. 7 Crystallographic structure (PDB code 4Z7U) of the T-lymphocyte receptor composed of α and β chains (green and yellow cartoons, respectively) interacting with the DQ8-glia-α1 peptide (shown with the stick representation). Electrostatic surface (+5 kT e^{-1}) obtained by the APBS tool[30] is shown. Peptide residues closest to the receptor surface are labelled. The figure was prepared by using the PyMOL program.

A visual analysis of the crystallographic structures allowed us to further select the residues to mutate and to select the possible mutations to be applied to these residues. In particular, among the residues in red, it was decided not to mutate the residues S1, G2 and N12, as they were positioned far from the receptor residues (Fig. 7). For the residues G4, S5, Q7, Q10 and P13, a total of 64 mutations were selected on the basis of the nature of the receptor residues located in their immediate vicinity. For example, G4 was located near a region of the receptor characterized by basic residues (shown in blue in Fig. 7), thus mutations towards negatively charged residues, such as D or E, were excluded for this residue.

Simulations were performed by mutating the residues G4, S5, Q7, Q10 and P13 of the peptide M1. For each simulation, the interaction energy of the peptide with both DQ8 (α and β chains) and with the T lymphocyte receptor (α and β chains) was calculated. Results are shown in Fig. 8a and b, for the two receptors S13 and L3–12, whose crystal structures were taken from the PDB models 4Z7U and 4Z7W, respectively. The most promising mutations were those whose representative points were positioned in the upper left quadrant (in Fig. 8, quadrants are delimited by the dotted lines passing through the reference peptide M1) of each plot, that is the quadrant including the peptide showing an enhanced interaction with DQ8 and a worsened interaction with the T-cell receptor with respect to M1. In this perspective, favourable mutations were found for residues S5, Q7, and Q10; in fact, S5R, Q7R and Q10I allow to optimize the anti-binding performance of the peptide with respect to both the S13 and L3–12 T-cell receptors, without substantially modifying its binding properties with DQ8.

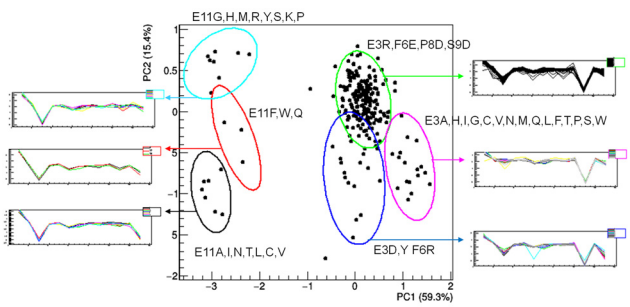

Fig. 6 Score plot of the first two principal components PC1 and PC2, calculated by PCA of the residue-by-residue interaction energy profiles for the DQ8-glia-α1 peptide. The percentage of data variance explained by each of the components is reported on their respective axes. 95% probability ellipses show the result of a hierarchical clustering procedure applied to the representative points. The insets show the superposed energy profiles for each cluster.

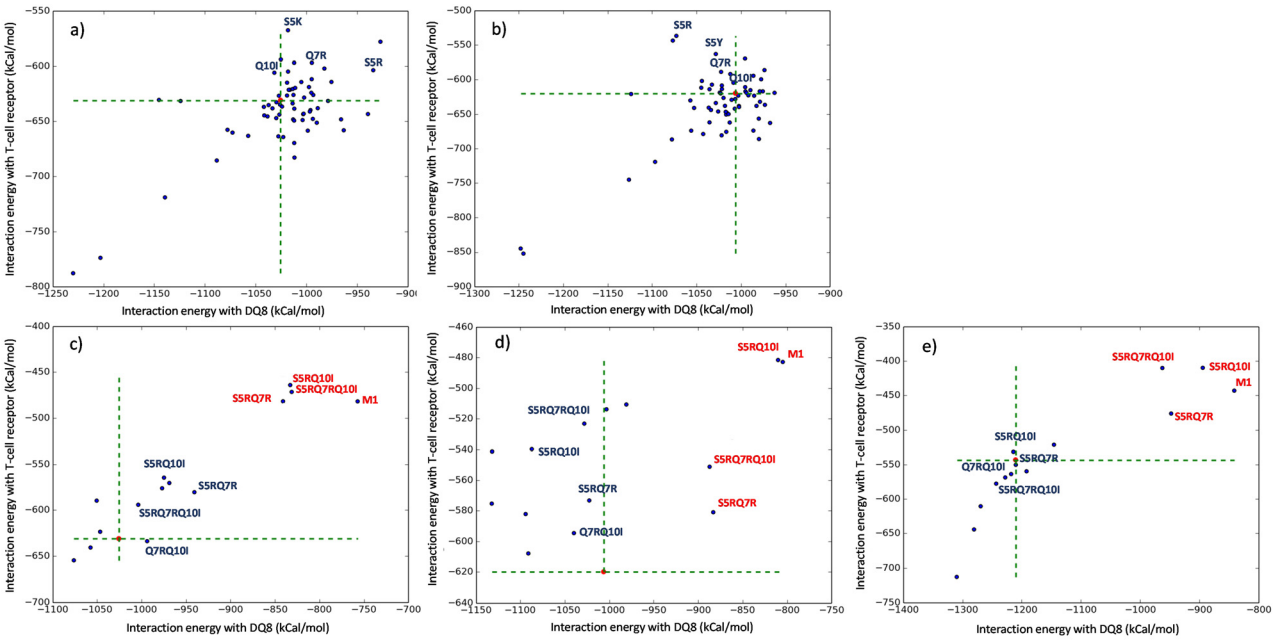

Fig. 8 Interaction energy values, averaged along the simulation, between the DQ8-glia-α1 peptide and the DQ8 protein, on the abscissa, of the S13 (a and c), L3–12 (b and d) and Bel502 (e) receptors, on the ordinate. Each point represents a simulation, performed by mutating one of the residues of DQ8-glia-α1. The red point represents the peptide optimized with respect to the binding properties with DQ8 (M2). It is taken as a reference to evaluate the energy variations of the introduced mutations (dashed lines). In a and b are reported the mutations of peptide residues not involved in strong interactions with DQ8: G4, S5, Q7, Q10 and P13. In c, d and e are reported multiple mutations applied to the M1 peptide. Here, the points labelled in red refer to the mutations performed on the DQ8-glia-α1 peptide.

The effect of these mutations, performed in a combined manner on the residues involved, was verified by performing further simulations of the optimized peptide M2, DQ8 and T-cell receptor. In addition to the two receptors already considered (S13 and L3–12), the study on these multiple mutations was also performed on the Bel502 receptor, whose crystal structure was taken from the PDB model 5KS9, in order to validate the procedure on a system not used for the analysis of single mutations. Furthermore, multiple mutations were also applied to the DQ8-glia-α1 peptide (M1), in order to verify their effect on binding with DQ8 also for this peptide.

The results shown in Fig. 8 highlight that the optimized peptide M2 has systematically better properties than the M1 peptide with regard to the interaction with DQ8. In fact, the interaction energy with DQ8 of M2 and its mutations were always lower than those of M1 and its mutations, even if this difference was reduced by not considering the role of the solvation waters (Fig. 8c, d and e). However, it was observed that the optimized peptide also had a lower interaction energy with the receptor than the native peptide, and this difference was preserved by applying multiple mutations. Furthermore, Fig. 8 shows that the S5R, Q7R and Q10I mutations present interesting additive properties, that is, their effect was additive if used in combination, and in general goes in the direction of decreasing the interaction energy with DQ8 and increasing that with the receptor. This property was observed equally on the optimized peptide and on the M1 one.

3.1.4 Improvement of the peptide design. Fig. 4 shows that mutations toward specific charged residues, *i.e.* E, D, K, and R, favour the interaction with DQ8. Calculations based on the molecular interaction fields, by using the GRID force field does not hold this bias and present differences compared to MD calculations, based on the CHARMM force field. In this regard, Fig. 9 shows the mutations that present low ΔE values for both CHARMM and GRID calculations by considering the peptide residues involved in the interaction with the DQ8

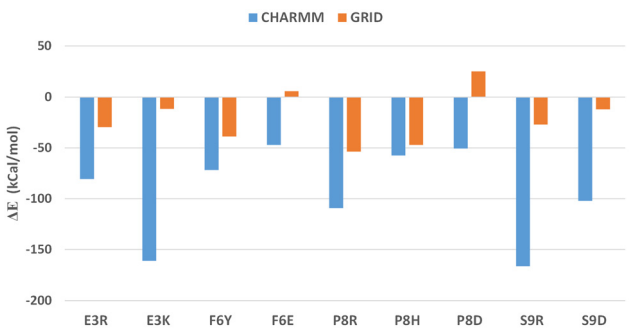

Fig. 9 Difference in the interaction energy ΔE calculated by using the CHARMM and GRID force fields for the system composed of the mutated DQ8-glia-α1 peptide and the DQ8 protein with respect to the energy observed for the system with the not-mutated DQ8-glia-α1 peptide.

protein. For the residue at position 3, the E3K mutation still presents negative ΔE values even for GRID calculations, even if it suggests that the E3R mutation is more appropriate. For the residue at position 6, the F6E mutation was not confirmed by the GRID calculation, as a positive ΔE value was obtained. For this residue, a consensus analysis between CHARMM and GRID calculations suggested that a F6Y mutation could be considered. For the residue at position 8, the GRID calculation returned a positive ΔE for P8D mutation, while the consensus analysis indicated that a mutation with a protonable residue such as arginine or histidine could be more appropriate. Finally, for the residue at position 9, the previous S9D mutation was disfavoured by the GRID calculation compared to the S9R mutation, as confirmed by the CHARMM calculation. Considering the need to reduce the number of *in vitro* tests on murine models, the mutations F6Y and P8R were selected, returning higher ΔE values in absolute value for both CHARMM and GRID force fields.

The list of peptides selected by the computational analysis is reported in Table 2, where the peptides M9 and M10 represent, respectively, the new peptide optimized for the interaction with DQ8 and the one optimized for the simultaneous interaction with DQ8 and anti-interaction with T cell receptors.

The reference peptide M2 was optimized for the interaction with DQ8, therefore it contains the mutations E3K, F6E, P8D and S9D (base peptide). Three variants of the M2 peptide were optimized for anti-interaction with the receptor. They contain the S5R, Q7R and Q10I mutations in addition to the previous ones. In particular, the combined mutations S5RQ10I, S5RQ7RQ10I and S5RQ7R, respectively, called R, R′ and R″, were selected. Ultimately, the R, R′ and R″ peptide variants were used to evaluate the anti-binding properties towards T-cell receptors of the parent peptide, while the Base + R, Base + R′ and Base + R″ peptide variants were used to evaluate the combined effect of an optimization for binding to DQ8 and anti-binding towards T-cell receptors.

3.2 Characterization of the synthesized peptides

The peptides reported in Table 3, which correspond to the DQ8-glia-α1 one (M1) plus those listed in Table 2, have been all synthesized at the level of milligrams, obtaining yields of around 30%. A glutamine was added at the C terminal of each peptide to avoid the presence of proline residues in this position that are especially prone to cause diketopiperazine formation, due to the basicity of their secondary amine.[35]

The HPLC and mass profiles of all the synthesized peptides are shown in Fig. S1 ESI.†

3.3 Evaluation of peptide stability in serum

Peptide degradation experiments were performed on M1, M5 and M10 in 10% human serum at 37 °C. The data are reported in Table 4 as the percentage of intact peptide over time obtained by integrating the peak area of the RP-HPLC profile.

The results obtained showed the stability of M1, M5 and M10 peptides over 8 h incubation with intact peptides of a per-

Table 2 List of mutations performed on the peptide DQ8-glia-α1. Mutations on residues E3, F6, P8 and S9 improve the interaction with DQ8, and those on residues S5, Q7 and Q10 hinder the interaction with T-cell receptors

Id	Description	Mutations
M2	Base	E3K, F6K, P8D, S9D
M3	R	S5R, Q10I
M4	Base + R	E3K, F6K, P8D, S9D + S5R, Q10I
M5	Base + R′	E3K, F6K, P8D, S9D + S5R, Q7R, Q10I
M6	R′	S5R, Q7R, Q10I
M7	Base + R″	E3K, F6K, P8D, S9D + S5R, Q7R
M8	R″	S5R, Q7R
M9	Base′	F6Y, P8R
M10	Base′ + R′	F6Y, P8R + S5R, Q7R, Q10I

Table 4 Peptide degradation evaluated over 48 h incubation in 10% human serum at 37 °C

M1	M5	M10
% intact peptide		
100	100	100
99	96	95
98	90	90
80	89	83
75	83	69
73	82	60
65	78	0.4
51	—	—

Table 3 List of peptides synthesized for *in vivo* testing. Residues found in the interaction pockets with DQ8 (numbers with underbars) and with the T-cell receptor (numbers with overbars) are highlighted. Not-mutated residues are numbered with no bars

Id	1	2	$\underline{3}$	4	$\bar{5}$	$\underline{6}$	$\bar{7}$	$\underline{8}$	$\underline{9}$	$\overline{10}$	11	12	13	14
M1	S	G	E	G	S	F	Q	P	S	Q	E	N	P	Q
M2	S	G	K	G	S	E	Q	D	D	Q	E	N	P	Q
M3	S	G	E	G	R	F	Q	P	S	I	E	N	P	Q
M4	S	G	K	G	R	E	Q	D	D	I	E	N	P	Q
M5	S	G	K	G	R	E	R	D	D	I	E	N	P	Q
M6	S	G	E	G	R	F	R	P	S	I	E	N	P	Q
M7	S	G	K	G	R	E	R	D	D	Q	E	N	P	Q
M8	S	G	E	G	R	F	R	P	S	Q	E	N	P	Q
M9	S	G	E	G	S	Y	Q	R	S	Q	E	N	P	Q
M10	S	G	E	G	R	Y	R	R	S	I	E	N	P	Q

centage of 73%, 82% and 60%, respectively, that remained almost the same for M1 and M5 after 24 hours, but definitely decreased for M10, which was completely degraded. A full degradation of M5 peptide occurred in 48 h, after that no intact peptide was detectable anymore. In contrast, M1 peptide was still present (51%) even after 48 h. Although the stability of M5 and M10 peptides was not fully comparable to that of M1, it was nevertheless optimal since peptide uptake onto the APC surface occurred very quickly. The long-term stability of M1 peptide was to be expected as it was already a product of gliadin digestion by pepsin and trypsin.

3.4 *In vitro* tests on DQ8 mice

We evaluated the immune effects generated by the immunodominant DQ8-restricted M1 peptide and its derivatives (Table 3). To induce systemic sensitisation, mice were immunized intraperitoneally with M1, whereas the control mice were immunized with gliadin or not immunized. M1 immunization induced INF-γ secretion following the *in vitro* challenge of splenocytes with M1, as well as with gliadin (Fig. 10A, left panel). Interestingly, M1 immunization, but not gliadin immunization, also stimulated IL-10 secretion following *in vitro* challenge with M1 or gliadin (Fig. 10A, right panel). Furthermore, none of the M1 analogues was able to stimulate *in vitro* IFN-γ in M1-sensitised spleen cells (Fig. 10B).

Notably, co-incubation of M1 with each single analogue showed that the M1-specific secretion of IFN-y could not be suppressed by any tested analogue (Fig. 10C). To characterize further the M1-specific immune response in DQ8 mice, a multi-parametric assessment of the inducible cytokine pattern was performed. The analysis confirmed that the *in vitro* challenge with M1 stimulated the secretion of both IFN-γ and IL-10 in M1-sensitised splenocytes (Fig. 11). In addition, we found that M1 specifically increased the secretion of IL17a (Fig. 11), a marker of active CD,[33] whereas IL-21, which contributes to enhance the Th1 response in CD,[34] was undetectable (data not shown); both cytokines were involved in adaptive immunity. Interestingly, we also found a specific increase of IL-6 and TNF-α, which were mainly related to innate immunity (Fig. 11). Next, we focused on the ability of M1 analogues to hold, in the absence of IFN-γ secretion, the ability to stimulate IL-10 secretion, in consideration of its anti-inflammatory nature. The results showed heterogeneity in the response. However, among the different tested peptides, M5 appeared to elicit a more consistent secretion of IL-10, not significantly different from M1 (Fig. 12A). Next, we focused on analogues designed on the M5 peptide to detail the aminoacidic sequence associated with the anti-inflammatory properties. A multi-parametric test was performed on M1-specific splenocytes that confirmed the absence of INF-γ stimulation by all analogues (Fig. 12B). Interestingly, IL-10 secretion was better induced by M10. Furthermore, we found that M5 still induced secretion of IL-17A, whereas M5-derived peptides were unable to induce it. Also, the ability to stimulate the secretion of innate immunity cytokines was reduced, but not completely abolished in M5 and its derivatives (Fig. 12B).

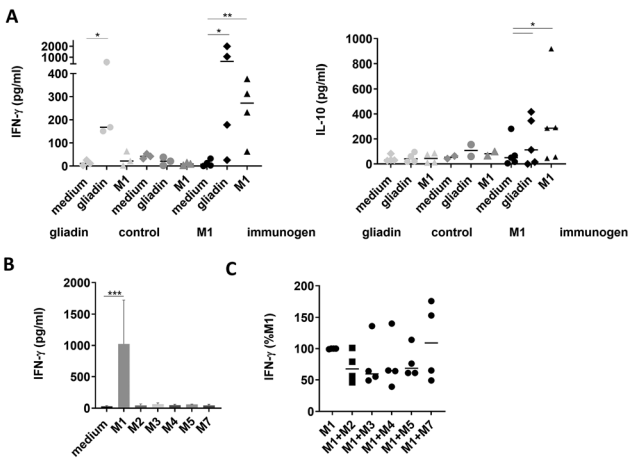

Fig. 10 ELISA analysis of IFN-γ and IL-10 secretions from splenocytes of DQ8 mice parenterally immunised with M1 peptide after 72 h stimulation *in vitro* (A). IFN-γ (left panel) and IL-10 (right panel) cytokines secreted following the challenge with pt-gliadin (gliadin), M1 or medium alone; the symbols represent means of duplicate values from a single mouse; the bars represent the medians (B). IFN-γ secreted following challenge with M1, M1 analogues or medium alone; the columns represent the means ± standard error of values from 5 mice per group. (C) IFN-γ secreted following the challenge with an equimolar amount of M1 + each analogue; the dots represent the means of duplicate values from a single mouse; the bars represent the medians. In (C), the medium values are subtracted. ***$P < 0.0001$; ** $P < 0.01$; *$P < 0.05$.

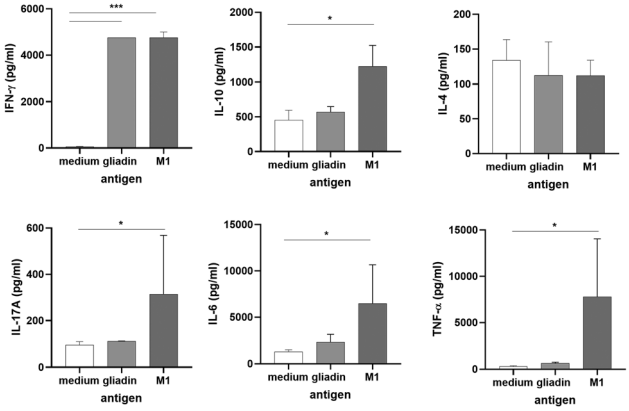

Fig. 11 Multi-parametric analysis of the secreted cytokines from the splenocytes of DQ8 mice parenterally immunised with M1 peptide after 72 h stimulation *in vitro* with wheat gliadin or M1. The columns represent the means ± standard error of values from 5 mice per group. ***$P < 0.01$; *$P < 0.05$.

4 Discussion

In this work, we analysed the down-regulation of the gliadin-specific inflammatory response in sensitized HLA-DQ8 transgenic (DQ8) mice and identified an anti-inflammatory analogue. Mice were from a colony bred for several generations on a GFD; therefore, they lacked the naturally induced immune tolerance toward gluten, similar to CD. To dissect the mecha-

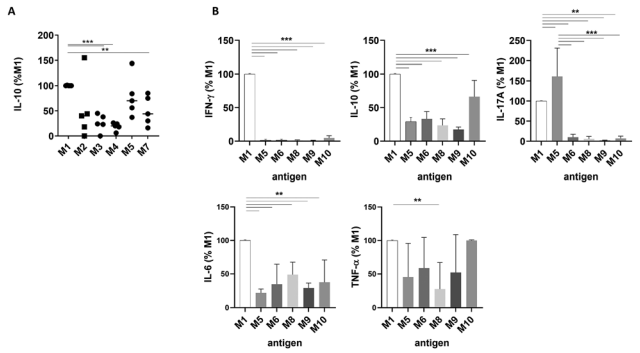

Fig. 12 (A) ELISA analysis of IL-10 secretion from the splenocytes of DQ8 mice parenterally immunised with M1 peptide following challenge with M1 or M5 analogues; the dots represent the means of duplicate values from a single mouse; the bars represent the medians. (B) Multi-parametric analysis of the secreted cytokines from the splenocytes of DQ8 mice parenterally immunised with M1 peptide after 72 h stimulation *in vitro* with M1, M5 or M5 analogues. The columns represent the means ± standard error of values from 5 mice per group. The medium values were subtracted. ***$P < 0.001$; **$P < 0.01$.

nisms underlying the immunomodulatory activity of M1-analogue peptides, we studied the *in vitro* recall response of the antigen-specific splenocytes. We found an important feature of M1 when used as an immunogen in contrast to whole gliadin, which was its ability to stimulate both pro- (IFN-γ) and anti-inflammatory (IL-10) secretions in spleen cells following an *in vitro* challenge with either antigens. This was instrumental in the perspective of designing analogues able to induce only an anti-inflammatory response. In the first round of screening, all M1 analogues showed a loss of the inflammatory capacity; however, we also found that they were non-M1 antagonists. In particular, we focused on the analogue M5 that elicited a significant secretion of IL-10. To more precisely identify the aminoacidic sequence responsible for the anti-inflammatory activity, a new series of analogues was synthesized and assessed. Interestingly, IL-10 secretion was better induced by M10. Another interesting property of M1, when used as an immunogen, was to stimulate *in vitro* the secretion of IL-17a, a multi-tasking cytokine of adaptive immunity, as well as of innate immunity markers (IL6 and TNF-α). IL-17a could inhibit the development of Th1 cells,[36] limiting the inhibitory effects of IFN-γ on Th17 development. Furthermore, Th17 cells could fully differentiate into Treg cells,[37] contributing to resolve an inflammatory condition. TNF-α is mainly produced by macrophages and classically promotes the inflammatory response. IL-6 has been associated with both pro- and anti-inflammatory effects.[38] Notably, IL-6 could induce the differentiation of naive T cells into inflammatory Th17 cells, characterized by IL-17a secretion,[39] which was the condition reported herein. Interestingly, secretions of IL-6 and TNF-α were induced by M1, but not by gliadin. Furthermore, this ability was still held by M5 and cognate analogues. Therefore, we speculated that this capacity was the consequence of the direct peptide binding onto the surface of antigen-presenting cells. In contrast, the secretion of IL17a was completely missed by all the M5 analogues, including M10.

5 Conclusions

Based on virtual mutagenesis studies, we designed and prepared nine new synthetic peptides derived from the gliadin HLA-DQ8-restricted immunodominant gliadin peptide M1. Their interaction energies, estimated with two complementary approaches, have been optimized to enhance their binding properties with DQ8 and their anti-binding properties with different human T-cell receptors. This latter feature was researched to avoid triggering the immune response typical of CD. These peptide candidates have been validated by a murine model already calibrated and used for CD studies. Immunological data confirmed the ability of the selected analogues to down-regulate the age-specific Th1/Th17 adaptive response, still preserving the ability to stimulate IL-10 secretion. Th1- and Th17-associated cytokines increased in the small intestinal mucosa of active CD.[40,41] In contrast, IL-10-producing cells were crucial in controlling TH1/Th17 responses to gliadin.[42] In particular, the results indicated the M10 peptide as a potential therapeutic molecule for down-regulating the inflammatory condition triggered by the DQ8-glia-α1 immunodominant peptide in CD.

Author contributions

Conceptualization: MR, ON, RC and MS. Formal analysis: RC, DT and BDB. Investigation: LT, RC, DT, FM, LZ, ADG and BDB. Methodology: VM, AGS and ON. Software: RC and DT. Writing – original draft: RC, LT, DT, AGS, FM, LZ and ADG. Writing – review & editing: BDB, RC, MS and MR.

Conflicts of interest

There are no conflicts to declare.

Data availability

Data for this article, including the PDB files of the atomistic models of the DQ8/DQ8-glia-α1 complex for each of the mutation applied to the peptide, are available at Zenodo (**https://doi.org/10.5281/zenodo.15004877**). In particular, the input models used for MD and the last MD frame used for the molecular interaction field calculations are stored.

Acknowledgements

This work was supported by the CNR project ALIFUN (PON MUR 2018, grant ARS01_00783) and by the Italian Ministry of University and Research under the National Recovery and

Resilience Plan (PRR.AP022.004 SPOKE3 PE10 CUP B83C22004790001, ON Foods). We acknowledge the Italian Bioinformatic Infrastructure ELIXIR-IIB for awarding access to the high-performance computing resources of CINECA (Italy) through the project entitled: "Identification of antagonists of gliadin peptides". The authors want to thank Mr Giorgio Varriale and Mr Massimiliano Mazzucchi for their technical support.

References

1 V. Abadie, A. S. Han, B. Jabri and L. M. Sollid, New Insights on Genes, Gluten, and Immunopathogenesis of Celiac Disease, *Gastroenterology*, 2024, **167**, 4–22.
2 Ò. Molberg, S. N. Mcadam, R. Körner, H. Quarsten, C. Kristiansen, L. Madsen, L. Fugger, H. Scott, O. Norén, P. Roepstorff, K. E. Lundin, H. Sjöströmm and L. M. Sollid, Tissue transglutaminase selectively modifies gliadin peptides that are recognized by gut-derived T cells in celiac disease, *Nat. Med.*, 1998, **4**, 713–717.
3 S. Senger, F. Maurano, M. F. Mazzeo, M. Gaita, O. Fierro, C. S. David, R. Troncone, S. Auricchio, R. A. Siciliano and M. Rossi, Identification of immunodominant epitopes of alpha-gliadin in HLA-DQ8 transgenic mice following oral immunization, *J. Immunol.*, 2005, **175**, 8087–8095.
4 F. Maurano, V. Rotondi Aufiero, L. Treppiccione, S. Rossi, D. Luongo, G. Mazzarella and M. Rossi, The HLA-DQ8 transgenic mouse: A model to study the immune and cytotoxic responses to wheat gliadin, *Methods Cell Biol.*, 2023, **179**, 157–171.
5 K. E. Black, J. A. Murray and C. S. David, HLA-DQ determines the response to exogenous wheat proteins: a model of gluten sensitivity in transgenic knockout mice, *J. Immunol.*, 2002, **169**, 5595–6000.
6 L. W. Vader, A. de Ru, Y. Van der Wal., Y. M. C. Kooy, W. Benckhuijsen, M. L. Merin, J. W. Wouter Drijfhout, P. van Veelen and F. Koning, Specificity of tissue transglutaminase explains cereal toxicity in celiac disease, *J. Exp. Med.*, 2002, **195**, 643–649.
7 G. Mazzarella, M. Maglio, F. Paparo, G. Nardone, R. Stefanile, L. Greco, Y. van de Wal, Y. Kooy, F. Koning, S. Auricchio and R. Troncone, An immunodominant DQ8 restricted gliadin peptide activates small intestinal immune response in in vitro cultured mucosa from HLA-DQ8 positive but not HLA-DQ8 negative coeliac patients, *Gut*, 2003, **52**, 57–62.
8 J. Petersen, J. van Bergen, K. L. Loh, Y. Kooy-Winkelaar, D. X. Beringer, A. Thompson, S. F. Bakker, C. J. Mulder, K. Ladell, J. E. McLaren, D. A. Price, J. Rossjohn, H. H. Reid and F. Koning, Determinants of gliadin-specific T cell selection in celiac disease, *J. Immunol.*, 2015, **194**, 6112–6122.
9 J. Petersen, Y. Kooy-Winkelaar, K. L. Loh, M. Tran, J. van Bergen, F. Koning, J. Rossjohn and H. H. Reid, Diverse T Cell Receptor Gene Usage in HLA-DQ8-Associated Celiac Disease Converges into a Consensus Binding Solution, *Structure*, 2016, **24**, 1643–1657.
10 P. Emsley and K. Cowtan, Model-Building Tools for Molecular Graphics, *Acta Crystallogr., Sect. D:Biol. Crystallogr.*, 2004, **60**, 2126–2132.
11 M. F. Gómez Castro, E. Miculán, M. G. Herrera, C. Ruera, F. Perez, E. D. Prieto, E. Barrera, S. Pantano, P. Carasi and F. G. Chirdo, Gliadin Peptide Forms Oligomers and Induces NLRP3 Inflammasome/Caspase 1-Dependent Mucosal Damage in Small Intestine, *Front. Immunol.*, 2019, **10**, 31.
12 M. J. Amundarain, A. Vietri, V. I. Dodero and M. D. Costabel, IDP Force Fields Applied to Model PPII-Rich 33-mer Gliadin Peptides, *J. Phys. Chem. B*, 2023, **127**, 2407–2417.
13 J. C. Phillips, R. Braun, W. Wang, J. Gumbart, E. Tajkhorshid, E. Villa, C. Chipot, R. D. Skeel, L. Kalé and K. Schulten, 2005. Scalable molecular dynamics with NAMD, *J. Comput. Chem.*, 2005, **26**, 1781–1802.
14 R. B. Best, X. Zhu, J. Shim, P. E. M. Lopes, J. Mittal, M. Feig and A. D. MacKerell, Optimization of the Additive CHARMM All-Atom Protein Force Field Targeting Improved Sampling of the Backbone ϕ, ψ and Side-Chain χ 1 and χ 2 Dihedral Angles, *J. Chem. Theory Comput.*, 2012, **8**, 3257–3273.
15 D. Beglov and B. Roux, Finite representation of an infinite bulk system: Solvent boundary potential for computer simulations, *J. Chem. Phys.*, 1994, **100**, 9050–9063.
16 W. L. Jorgensen, J. Chandrasekhar, J. D. Madura, R. W. Impey and M. L. Klein, Comparison of simple potential functions for simulating liquid water, *J. Chem. Phys.*, 1983, **79**, 926–935.
17 T. Darden, D. York and L. Pedersen, Particle mesh Ewald: An N·log(N) method for Ewald sums in large systems, *J. Chem. Phys.*, 1993, **98**, 10089–10092.
18 H. C. Andersen, Rattle: A "velocity" version of the shake algorithm for molecular dynamics calculations, *J. Comput. Phys.*, 1983, **52**, 24–34.
19 S. Nosé and M. L. Klein, Constant pressure molecular dynamics for molecular systems, *Mol. Phys.*, 1983, **50**, 1055–1076.
20 H. C. Andersen, Molecular dynamics simulations at constant pressure and/or temperature, *J. Chem. Phys.*, 1980, **72**, 2384–2393.
21 M. Parrinello and A. Rahman, Polymorphic transitions in single crystals: A new molecular dynamics method, *J. Appl. Phys.*, 1981, **52**, 7182–7190.
22 Schrödinger, LLC, *The PyMOL Molecular Graphics System, Version 1.8*, 2015.
23 W. Humphrey, A. Dalke and K. Schulten, VMD: Visual molecular dynamics, *J. Mol. Graphics*, 1996, **14**, 33–38.
24 T. Castrignanò, S. Gioiosa, T. Flati, M. Cestari, E. Picardi, M. Chiara, M. Fratelli, S. Amente, M. Cirilli, M. A. Tangaro, G. Chillemi, G. Pesole and F. Zambelli, ELIXIR-IT HPC@CINECA: high performance computing resources for the bioinformatics community, *BMC Bioinf.*, 2020, **21**, 352.

25 A. Mazzone, M. Lopresti, B. D. Belviso and R. Caliandro, New features of the RootProf program for model-free analysis of unidimensional profiles, *J. Appl. Crystallogr.*, 2023, **56**, 1841–1854.
26 D. Trisciuzzi, L. Siragusa, M. Baroni, I. Autiero, O. Nicolotti and G. Cruciani, Getting Insights into Structural and Energetic Properties of Reciprocal Peptide–Protein Interactions, *J. Chem. Inf. Model.*, 2022, **62**, 1113–1125.
27 P. J. Goodford, A computational procedure for determining energetically favorable binding sites on biologically important macromolecules, *J. Med. Chem.*, 1985, **28**, 849–857.
28 D. Trisciuzzi, L. Siragusa, M. Baroni, G. Cruciani and O. Nicolotti, An Integrated Machine Learning Model To Spot Peptide Binding Pockets in 3D Protein Screening, *J. Chem. Inf. Model.*, 2022, **62**(24), 6812–6824.
29 P. L. Weegels, R. J. Hamer and J. D. Schofield, RP-HPLC and capillary electrophoresis of subunits from glutenin isolated by SDS and Osborne fractionation, *J. Cereal Sci.*, 1995, **22**, 211–224.
30 E. Jurrus, D. Engel, K. Star, K. Monson, J. Brandi, L. E. Felberg, D. H. Brookes, L. Wilson, J. Chen, K. Liles, M. Chun, P. Li, D. W. Gohara, T. Dolinsky, R. Konecny, D. R. Koes, J. E. Nielsen, T. Head-Gordon, W. Geng, R. Krasny, G.-W. Wei, M. J. Holst, J. A. McCammon and N. A. Baker, Improvements to the APBS biomolecular solvation software suite, *Protein Sci.*, 2018, **27**, 112–128.
31 J. Petersen, Y. Kooy-Winkelaar, K. L. Loh, M. Tran, J. van Bergen, F. Koning, J. Rossjohn and H. H. Reid, Diverse T Cell Receptor Gene Usage in HLA-DQ8-Associated Celiac Disease Converges into a Consensus Binding Solution, *Structure*, 2016, **24**, 1643–1657.
32 K. N. Henderson, J. A. Tye-Din, H. H. Reid, Z. Chen, N. A. Borg, T. Beissbarth, A. Tatham, S. I. Mannering, A. W. Purcell, N. L. Dudek, D. A. van Heel, J. McCluskey, J. Rossjohn and R. P. Anderson, A Structural and Immunological Basis for the Role of Human Leukocyte Antigen DQ8 in Celiac Disease, *Immunity*, 2007, **27**, 23–34.
33 E. Aghamohamadi, N. Asri, A. Odak, M. Rostami-Nejad, V. Chaleshi, Y. Hajinabi, M. Eslami, S. Mohammadian Haftcheshmeh, F. S. Gholam-Mostafaei, H. Asadzadeh-Aghdaei, A. Masotti and M. R. Zali, Gene expression analysis of intestinal IL-8, IL-17 A and IL-10 in patients with celiac and inflammatory bowel diseases, *Mol. Biol. Rep.*, 2022, **49**, 6085–6091.
34 M. Sarra, M. Cupi, I. Monteleone, E. Franzè, G. Ronchetti, A. Di Sabatino, P. Gentileschi, L. Franceschilli, P. Sileri, G. Sica, G. Del Vecchio Blanco, M. Cretella, O. A. Paoluzi, G. R. Corazza, F. Pallone and G. Monteleone, IL-15 positively regulates IL-21 production in celiac disease mucosa, *Mucosal Immunol.*, 2013, **6**, 244–255.
35 Y. Yang, *Side Reactions in Peptide Synthesis*, Academic Press, 2015. ISBN: 978-0-12-801009-9.
36 S. Nakae, Y. Iwakura, H. Suto and S. J. Galli, Phenotypic differences between Th1 and Th17 cells and negative regulation of Th1 cell differentiation by IL-17, *J. Leukocyte Biol.*, 2007, **81**, 1258–1268.
37 N. Gagliani, M. C. Amezcua Vesely, A. Iseppon, L. Brockmann, H. Xu, N. W. Palm, M. R. de Zoete, P. Licona-Limón, R. S. Paiva, T. Ching, C. Weaver, X. Zi, X. Pan, R. Fan, L. X. Garmire, M. J. Cotton, Y. Drier, B. Bernstein, J. Geginat, B. Stockinger, E. Esplugues, S. Huber and R. A. Flavell, Th17 cells transdifferentiate into regulatory T cells during resolution of inflammation, *Nature*, 2015, **523**, 221–225.
38 J. Scheller, A. Chalaris, D. Schmidt-Arras and S. Rose-John, The pro- and anti-inflammatory properties of the cytokine interleukin-6, *Biochim. Biophys. Acta*, 2011, **1813**, 878–888.
39 A. Kimura and T. Kishimoto, IL-6: regulator of Treg/Th17 balance, *Eur. J. Immunol.*, 2010, **40**, 1830–1835.
40 A. Castellanos-Rubio, I. Santin, I. Irastorza, L. Castano, J. Carlos Vitoria and J. Ramon Bilbao, TH17 (and TH1) signatures of intestinal biopsies of CD patients in response to gliadin, *Autoimmunity*, 2009, **42**, 69–73.
41 I. Monteleone, M. Sarra, G. Del Vecchio Blanco, O. A. Paoluzi, E. Franzè, D. Fina, A. Fabrizi, T. T. MacDonald, F. Pallone and G. Monteleone, Characterization of IL–17A–producing cells in celiac disease mucosa, *J. Immunol.*, 2010, **184**, 2211–2218.
42 L. Passerini, G. Amodio, V. Bassi, S. Vitale, I. Mottola, M. Di Stefano, L. Fanti, P. Sgaramella, C. Ziparo, S. Furio, R. Auricchio, G. Barera, G. Di Nardo, R. Troncone, C. Gianfrani and S. Gregori, IL-10-producing regulatory cells impact on celiac disease evolution, *Clin. Immunol.*, 2024, **260**, 109923.